Intensity of singular stress fields of an embedded fibre under pull-out force

Intensity of singular stress fields of an embedded fibre under pull-out force

IOP Conf. Series: Materials Science and Engineering **369** (2018) 012003 doi:10.1088/1757-899X/369/1/012003

Intensity of singular stress fields of an embedded fibre under pull-out force

D Chen[1], G W Zhang[1], R Takaki[1], A Inoue[1], K Tsuboi[1], Y Sano[1] and N-A Noda[1,2]

[1]Department of Mechanical and Control Engineering, Kyushu Institute of Technology Sensui-Cho 1-1 Tobata-Ku, Kitakyushu-Shi, Fukuoka, Japan

E-mail: noda@mech.kyutech.jp

Abstract. Previous experimental studies of fibre pull-out test show two dangerous points on the interface. Failure usually occurs at the bonded end of the fibre (Point A) or at the entry point on the surface of the matrix (Point E). Both points have different singular stress fields which causes crack initiation, crack propagation, and final failure. In this paper, intensity of singular stress fields (ISSF) at the fibre bonded end A and ISSF at the intersection point E of the fibre and the surface are discussed. The analysis method focuses on calculating the finite element method (FEM) stress radio by using a reference model and an unknown model. In the unknown model and the reference model, same FEM mesh pattern is applied. To analyse the ISSF at A, the body force method solution is used as the reference model. To analyse the ISSF at E, the reciprocal work contour integral method (RWCIM) solution is used as the reference model. Then, the two ISSFs are compared and discussed by varying the fibre embedded length l_{in}. When l_{in} is shorter, the singular stress at A is larger than the singular stress at E. When l_{in} is longer, the singular stress at E is larger than the ISSF at A.

1. Introduction

Fibre reinforced composites are very common nowadays in construction, marine industry, aerospace technology, transportation sector, consumer products and industrial equipment [1-4]. In fibre reinforced composites, fibres are mainly used to enhance load carrying capacity. Indeed, composites are produced when two or more materials or phases are used together to give a combination of properties that cannot be achieved otherwise [4]. The mechanical properties of fibre-reinforced plastics are governed, to a great extent, by the adhesion of the matrix to the fibre surface, i.e. the interface bond strength [5]. Many different alternative test set-ups and experimental techniques have been developed in recent years to gain more insight into the basic mechanisms dominating the properties of the fibre/matrix interface. One of the most popular is the pull-out test in which a single fibre or bar is pulled out off the surrounding matrix and the corresponding load versus displacement relation, $P(\omega)$, is recorded [6]. However, the inhomogeneous stress distribution on the interface with stress concentrations at the fibre entry point and at the fibre bonded end cannot be indicated by $P(\omega)$. The resistance $P(\omega)$of the debonding and pull-out processes depends on the bond properties of the fibre/matrix interface and the interfacial bond area. Commonly, the failure is assumed to occur when the maximum load is reached. However, pull-out experiments revealed that the interface crack forms long before the maximum load is reached [7]. Besides, a typical force-displacement curve from the pull-out test was shown. The ‘kink’ in the figure indicates crack initiation [8].

S Zhandarov *et al* found the $P(\omega)$ curve of pull-out and micro-bond tests is similar, i.e. crack

propagation may starts from the fibre entry point E [8-10]. However, K-H Tsai *et al* observed that crack initiate at the fibre bonded end A during the fibre pull-out test [11,12]. In a rod pull out test that very similar to fibre pull-out test, C. Atkinson, et al. observed crack initiation sometimes occur at point A and sometimes occur at Point E [13].

2-D analytical model for the embedded fibre under pull-out force is shown in figure 1. As mentioned above, stress singularities arise at the fibre entry point E as well as at the fibre bonded end A in the theory of elasticity under idealized geometrical conditions, i.e. at sharp transitions between the two phases, even though no interface crack has formed [7]. The order of singularity arising at Point A and at Point E is not constant, but varies with the angle between the two surfaces as well with the elastic constants of fibre and matrix. The determination of stress intensity factors (i.e. ISSF) remains reserved to the analysis of an interface crack, even though the situation is more complex compared with the homogeneous case [7]. There are two different types of specific singular stress fields at point A as well as at point E. However, little research on these two singular stress fields is found. Therefore, attention is paid to discuss the ISSF by varying the fibre bonded length l_{in}.

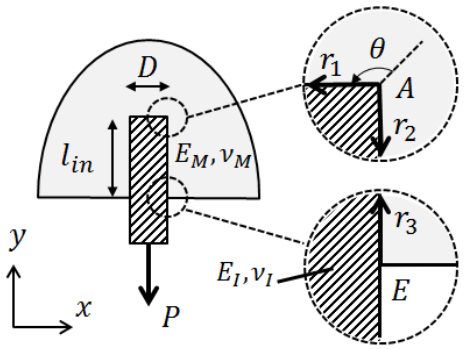

Figure 1. Reinforcing fibre under pull-out force.

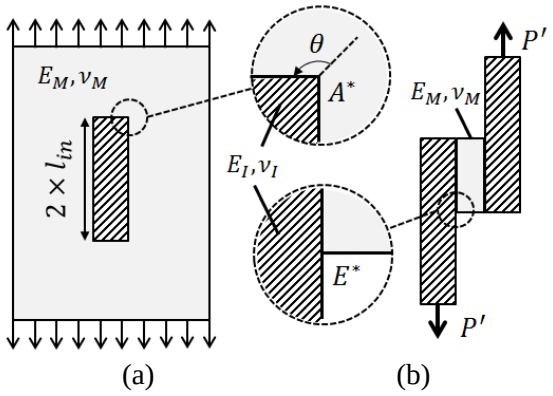

Figure 2. (a) Rectangular inclusion in infinite plate and (b) Single lap joint.

As is shown in figure 2(a), a rectangular inclusion is embedded in an infinite matrix under tension. Since the stress concentration zone is very small compared with the fibre diameter, the singular stress field at point A in Figure 1 is similar to that at point A^* in figure 2. Therefore, configuration shown in figure 2(a) can be used as the reference problem of the fibre bond end. The order of singularity arising at point A^* was discussed by D H Chen *et al* [14-16] Singular stress field at point E in figure 1 and at point E^* in figure 2 is similar. As is shown in figure 2(b), Point E^* is the corner of the interface of a single lap joint, at which ISSF was discussed by Miyazaki *et al* [17,18]. The singular stress field in this case can be examined by the interaction line integral method (RWCIM method) [19].

2. The two specific singular stress fields

As the order of singularity arising at point A and at point E is different, the singular stress field at point A and at point E has to be calculated separately.

2.1. Singular stress around corner A

On the one hand, stress distribution near corner A can be expressed as follows [14-16,20]:

$$\sigma_{ij,k} = \frac{K^A_{I,\lambda^A_1}}{r^{1-\lambda^A_1}} f^I_{ij,k}(\theta) \pm \frac{K^A_{II,\lambda^A_2}}{r^{1-\lambda^A_2}} f^{II}_{ij,k}(\theta) \qquad (ij = r,\theta,r\theta;\ k = M,I\ ) \tag{1}$$

In order to calculate the normal stress $\sigma^A_y(r_1)$ on the interface r_1, $ij = \theta$ and $\theta = 3\pi/4$ are used as shown in figure 1. Similarly, normal stress $\sigma^A_x(r_2)$ on the interface r_1 can be calculated from equation

(1) when $\theta = -3\pi/4$. Here, $f_{ij,k}^{I}(\theta)$ and $f_{ij,k}^{II}(\theta)$ can be calculated from equation (2) [14-16]. $K_{I,\lambda_1^A}^{A}$ and $K_{II,\lambda_2^A}^{A}$ are ISSFs, which are used for mode I and Mode II failure seperately. $K_{\sigma,\lambda_1^A}^{A} = K_{I,\lambda_1^A}^{A} \cdot f_{ij,k}^{I}(\theta)$ and $K_{\sigma,\lambda_2^A}^{A} = K_{II,\lambda_2^A}^{A} \cdot f_{ij,k}^{II}(\theta)$.

For matrix M ($-3\pi/4 \le \theta \le 3\pi/4$) [15,16]

$$\begin{aligned} f_{\theta,M}^{I}(\theta) = \frac{\lambda_1^A}{\sqrt{2\pi}(\alpha-\beta)}\{&[-\lambda_1^A(\alpha-\beta)\,cos(\lambda_1^A\pi/2) + (1-\beta)\,sin(\lambda_1^A\pi)] \times cos[(\lambda_1^A+1)\theta]\} \\ &+(\lambda_1^A+1)(\alpha-\beta)sin(\lambda_1^A\pi/2) \times cos[(\lambda_1^A-1)\theta] \\ f_{\theta,M}^{II}(\theta) = \frac{\lambda_2^A}{\sqrt{2\pi}(\alpha-\beta)}\{&\left[-\lambda_2^A(\alpha-\beta)\,cos\left(\lambda_2^A\pi/2\right) - (1-\beta)\,sin\left(\lambda_2^A\pi\right)\right] \times sin\left[\left(\lambda_2^A+1\right)\theta\right]\} \\ &+(\lambda_2^A+1)(\alpha-\beta)sin(\lambda_2^A\pi/2) \times sin\left[\left(\lambda_2^A-1\right)\theta\right] \end{aligned} \tag{2}$$

Here, α, βdenote Dundurs bimaterial parameters, and shear modulus G_I and G_M can be transformed from Young's Modulus E_I, E_M and Poisson's Ratio ν_I and ν_M.

$$\alpha = \frac{G_M(\kappa_I+1)-G_I(\kappa_M+1)}{G_M(\kappa_I+1)+G_I(\kappa_M+1)} \qquad \beta = \frac{G_M(\kappa_I-1)-G_I(\kappa_M-1)}{G_M(\kappa_I+1)+G_I(\kappa_M+1)}$$

$$\kappa_i = \begin{cases} (3-\nu_i)/(1+\nu_i) & (Plain\ stress) \\ (3-4\nu_i) & (Plain\ strain) \end{cases} \qquad (i = M, I) \tag{3}$$

Singular indexes λ_1^A, λ_2^A around the corner A can be calculated from the following equations (4) [15]. Here, the singular indexes λ_1^A, λ_2^A have real values in the range ($0 < \mathrm{Re}(\lambda_i^A) < 1$) if $\beta(\alpha-\beta) > 0$, which are equivalent to the order of singularity. Here, $\gamma = \pi/2$.

$$\begin{aligned} D_1(\alpha,\beta,\gamma,\lambda) &= (\alpha-\beta)^2\lambda^2[1-cos(2\gamma)] + 2\lambda(\alpha-\beta)sin(\gamma)\{sin(\lambda\gamma) + sin[\lambda(2\pi-\gamma)]\} \\ &+2\lambda(\alpha-\beta)\beta\cdot sin(\gamma)\{sin[\lambda(2\pi-\gamma)] - sin(\lambda\gamma)\} \\ &+(1-\alpha^2) - (1-\beta^2)cos(2\lambda\pi) + (\alpha^2-\beta^2)\,cos[2\lambda(\gamma-\pi)] = 0 \\ D_2(\alpha,\beta,\gamma,\lambda) &= (\alpha-\beta)^2\lambda^2(1-cos2\gamma) - 2\lambda(\alpha-\beta)sin(\gamma)\{sin(\lambda\gamma) + sin[\lambda(2\pi-\gamma)]\} \\ &-2\lambda(\alpha-\beta)\beta\cdot sin(\gamma)\{sin[\lambda(2\pi-\gamma)] - sin(\lambda\gamma)\} \\ &+(1-\alpha^2) - (1-\beta^2)cos(2\lambda\pi) + (\alpha^2-\beta^2)\,cos[2\lambda(\gamma-\pi)] = 0 \end{aligned} \tag{4}$$

2.2. Singular stress around corner E

On the other hand, singular stress distribution around the corner E along the interface r_3, as is shown in figure 1, can be expressed as follows [17,18]:

$$\sigma_x^E(r) = \frac{K_{\sigma,\lambda_1^E}^{E}}{r^{1-\lambda_1^E}} + \frac{K_{\sigma,\lambda_2^E}^{E}}{r^{1-\lambda_2^E}} \tag{5}$$

The value of singular index λ_1^E and λ_2^E can be determined from equation (6) [20-22]. Detail calculation of $K_{\sigma,\lambda_1^E}^{E}$ and $K_{\sigma,\lambda_2^E}^{E}$in reference problem can be found in [17,18].

$$\begin{aligned} &4sin^2(\pi\lambda)\left\{sin^2\left(\frac{\pi\lambda}{2}\right) - \lambda^2\right\}\beta^2 + 4\lambda^2sin^2(\pi\lambda)\alpha\beta + \left\{sin^2\left(\frac{\pi\lambda}{2}\right) - \lambda^2\right\}\alpha^2 - 4\lambda^2sin^2(\pi\lambda)\beta \\ &-2\left\{\lambda^2\,cos(2\pi\lambda) + sin^2\left(\frac{\pi\lambda}{2}\right)cos(\pi\lambda) + \frac{1}{2}sin^2(\pi\lambda)\right\}\alpha + sin^2\left(\frac{3\pi\lambda}{2}\right) - \lambda^2 = 0 \end{aligned} \tag{6}$$

2.3. Singular index of different material combinations

Some results of singular index from equation (4) and equation (6) are shown in table 1. It can be verified that the singularity arising at point A and at point E is different.

Table 1. Singular index λ value for some material combination.

	λ_1^A	λ_2^A	λ_1^E	λ_2^E
$\alpha = -0.90 \quad \beta = -0.40$	0.752493	0.748645	0.800102	0.997323
$\alpha = -0.90 \quad \beta = -0.20$	0.796059	0.699861	0.657967	0.999111
$\alpha = -0.80 \quad \beta = -0.40$	0.772894	0.847628	0.794890	0.988598
$\alpha = -0.80 \quad \beta = -0.20$	0.809649	0.791916	0.651598	0.996246
$\alpha = -0.9071 \quad \beta = -0.2016$	0.763235	0.621844	0.659165	0.999232

3. Method of analysis

Finite Element Method (FEM) was widely used for many engineering applications [23-28]. In this analysis software MSC Marc was used. Stress distribution along the interface (r_1, r_2, r_3) were calculated by applying the same mesh pattern to the pull-out model and reference model. Thus stress ratio $\left[\sigma^{\mathrm{A}}_{I,FEM}(r)/\sigma^{\mathrm{A}*}_{I,FEM}(r)\right]$ can be calculated between the pull-out model and the reference model. Similar method was used in [17,18].

As is shown in equation (7), $\sigma^A_{I,FEM}(r)$ is calculated from the stress distribution $\sigma_y^A(r_1)$ along the interface r_1 and $\sigma_x^A(r_2)$ along the interface r_2 by using the pull-out model (figure 1). $\sigma^{A*}_{I,FEM}(r)$ is calculated from the stress distribution $\sigma_y^{A*}(r_1)$ along the interface r_1 and $\sigma_x^{A*}(r_2)$ along the interface r_2 by using the reference model (figure 2). Material properties are shown in table 2. As mentioned above, Fibre in figure 1 and Inclusion in figure 2(b) are set to be same material properties.

$$2\sigma_I^A(r) = \sigma_y^A(r_1) + \sigma_x^A(r_2), (r = r_1 = r_2); \quad 2\sigma_{II}^A(r) = \sigma_y^A(r_1) - \sigma_x^A(r_2), (r = r_1 = r_2). \qquad (7)$$

Table 2. Material properties.

	Matrix Epon 828	Fibre (Inclusion) E-Glass
Young's Modulus	E_M = 3.3 GPa	E_I = 75 GPa
Poisson's Ratio	0.35	0.17

Table 3. FEM Stress Ratio of Symmetrical type.

Smallest mesh size $e_{min} = 3.8 \times 10^{-8}$			Smallest mesh size $e_{min} = 1.27 \times 10^{-8}$		
$\frac{r}{e_{min}}$	$\sigma^{\mathrm{A}}_{I,FEM}(r)$ [MPa]	$\frac{\sigma^{\mathrm{A}}_{I,FEM}(r)}{\sigma^{\mathrm{A}*}_{I,FEM}(r)}$	$\frac{r}{e_{min}}$	$\sigma^{\mathrm{A}}_{I,FEM}(r)$ [MPa]	$\frac{\sigma^{\mathrm{A}}_{I,FEM}(r)}{\sigma^{\mathrm{A}*}_{I,FEM}(r)}$
0.0	13.20	1.136	0.0	16.53	1.136
0.5	10.88	1.135	0.5	13.62	1.136
1.0	8.383	1.135	1.0	10.49	1.135
1.5	7.741	1.134	1.5	9.681	1.135
2.0	7.603	1.134	2.0	9.507	1.135

In order to verify that the stress ratio between reference model and pull-out model is independent of mesh size, different mesh size e_{min} is used. As shown in table 3, for different e_{min} the value of the symmetrical type stress $\sigma^{A}_{I,FEM}(r)$ is different, while the ratio of stress distribution $\left[\sigma^{A}_{I,FEM}(r)/\sigma^{A*}_{I,FEM}(r)\right]$ is constant. Same situation happen to $\sigma^{A}_{II,FEM}(r)$ and $\left[\sigma^{A}_{II,FEM}(r)/\sigma^{A*}_{II,FEM}(r)\right]$, which is known as Skew-symmetrical type.

The normalized stress intensity factor F_I^* and F_{II}^* can be acquired on the basis of body force method [14]. Here F_I^* and F_{II}^* of the reference problem can be expressed as follows, in which $l_2 = D/2$.

$$F_I^* = K^*_{I,\lambda_1^A}/(\sigma^\infty\sqrt{\pi}l_2^{1-\lambda_1^A}) \qquad F_{II}^* = K^*_{II,\lambda_2^A}/(\sigma^\infty\sqrt{\pi}l_2^{1-\lambda_2^A}) \tag{8}$$

The normalized stress intensity factor of the fibre pull-out problem can be defined similarly as follows:

$$F_I = K^A_{I,\lambda_1^A}/[(P/2l_2)\sqrt{\pi}l_2^{1-\lambda_1^A}] \qquad F_{II} = K^A_{II,\lambda_2^A}/[(P/2l_2)\sqrt{\pi}l_2^{1-\lambda_2^A}] \tag{9}$$

As is shown in equations (10), by using the FEM stress ratio mentioned above and F_I^* acquired by body force method, F_I for the fibre pull-out problem can be calculated. So is F_{II}.

$$\frac{F_I}{F_I^*} = \frac{\sigma^I_{\theta,FEM}(r)}{\sigma^{I*}_{\theta,FEM}(r)} \qquad \frac{F_{II}}{F_{II}^*} = \frac{\sigma^{II}_{\theta,FEM}(r)}{\sigma^{II*}_{\theta,FEM}(r)} \tag{10}$$

4. Numerical results and discussion

In short fibre reinforced composite, the aspect ratio $2l_{in}/D$ of short fibres is about 30 [29]. In this study, we assume the diameter of the fibre, i.e. the width of the inclusion, is D = 21 μm in the 2-D model. The total fibre length should be l = 630 μm . Therefore, the embedded length of the fibre l_{in}, from 30 μm to 1000 μm, was considered in the material combination shown in table 2.

4.1. ISSF at point A of different l_{in}

The ISSF values K^A_{σ,λ_1^A} and K^A_{σ,λ_2^A} correspond to λ_1^A and λ_2^A, respectively. It is found that, K^A_{σ,λ_1^A} and K^A_{σ,λ_2^A} decrease as the embedded length l_{in} increases.

For example when l_{in} = 150μm, K^A_{σ,λ_1^A} = 0.02334$MPa\cdot m^{1-0.7632}$, whereas when l_{in} = 300μm, K^A_{σ,λ_1^A} = 0.01494 $MPa\cdot m^{1-0.7632}$. The value of K^A_{σ,λ_1^A} for l_{in} = 300μm is 36.0% less than that of l_{in} = 150μm. Besides, when l_{in} = 150μm, K^A_{σ,λ_2^A} = 0.01519 $MPa\cdot m^{1-0.6218}$, whereas when l_{in} = 300μm, K^A_{σ,λ_2^A} = 0.01017 $MPa\cdot m^{1-0.6218}$. The value of K^A_{σ,λ_2^A} for l_{in} = 300μm is 33.0% less than that of l_{in} = 150μm. That is, the ISSF of the $1/2$ embedded case is about 2/3 of that of 1/4 embedded case.

4.2. ISSF at point E

The ISSF values K^E_{σ,λ_1^E} and K^E_{σ,λ_2^E} correspond to λ_1^E and λ_2^E, respectively. It is found that, K^E_{σ,λ_1^A} and K^E_{σ,λ_2^A} decrease as the embedded length l_{in} increases.

For example, when about 1/4 of the length of the fibre is embedded, l_{in} = 150μm, when about half of the fibre is embedded l_{in} = 300μm. When l_{in} = 150μm, K^E_{σ,λ_1^E} = 0.03689$MPa\cdot m^{1-0.6592}$, whereas when l_{in} = 300 μm, K^E_{σ,λ_1^E} = 0.03219 $MPa\cdot m^{1-0.6592}$. The value for l_{in} = 300μm is 12.7% less than that of l_{in} = 150 μm. Besides, when l_{in} = 150μm, K^E_{σ,λ_2^E} = -0.04929 $MPa\cdot m^{1-0.9992}$, whereas when l_{in} = 300 μm, $K^E_{\sigma,\lambda_2^E} = -0.05350\ MPa\cdot m^{1-0.9992}$. The value for l_{in} = 300μm is 8.54% less than that of l_{in} = 150 μm. That is, the ISSF of the $1/2$ embedded case is about 10% less than that of 1/4 embedded case.

4.3. Compare of ISSF at point A and at point E

As the singular indexes (λ_1^A, λ_2^A), (λ_1^E, λ_2^E) are different at point A and at point E, it is not possible to compare ISSF directly. In order to compare the magnitude of the ISSF at point A and at Point E. Before crack initiation the radial tensile stress greatly exceed the shear stresses [7,30]. Therefore, $\sigma_y^A(r_1)$ and $\sigma_x^E(r_3)$ is calculated from the ISSFs. Here, $\sigma_x^E(r_3)$ is the radial stress distribution along interface r_3 in figure 1. As is shown in figure 3 when l_{in} = 100μm, the peculiar stress at point A is larger than the specific stress at point E. Therefore, the crack initiation may occur from point A. However, figure 4 shows that when l_{in} = 1000μm, radial stress at point A is larger than the specific stress at point E, and crack initiation may occur from point E.

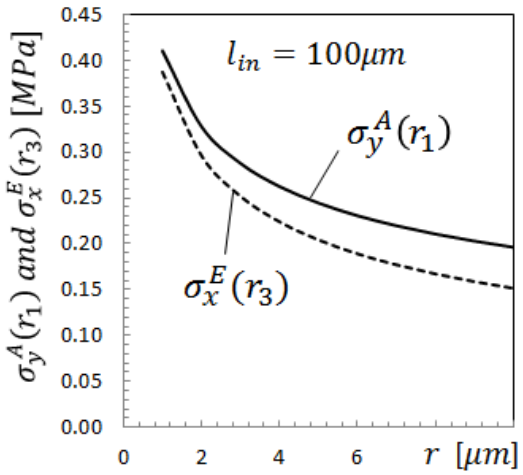

Figure 3. The dependence of $\sigma_y^A(r_1)$ and $\sigma_x^E(r_3)$ on r if $l_{in} = 100\mu m$

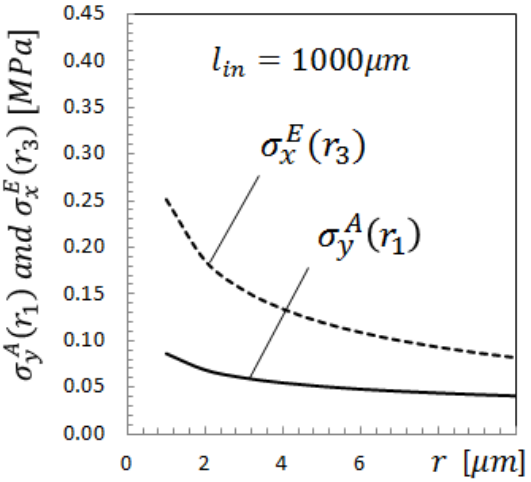

Figure 4. The dependence of $\sigma_y^A(r_1)$ and $\sigma_x^E(r_3)$ on r if $l_{in} = 1000\mu m$

5. Conclusions

In this study, the singular stress fields generated at the entry point and at the bond end of an embedded fibre under pull-out force are discussed. Stress distribution around the two areas was compared, and the following conclusions were obtained.

- The ISSF K^A_{σ,λ_1^A} and K^A_{σ,λ_2^A} at point A decreases as the embedded length l_{in} gets longer.
- The ISSF K^E_{σ,λ_1^E} *and* K^E_{σ,λ_2^E} at point E decreases as the embedded length l_{in} gets longer.
- For the selected material combination the singular stress at the entry point is larger than that at the bonded end if $l_{in} > 300$μm. On the other hand, the crack of embedded fibres may occur from bonded end if $l_{in} < 300$μm..

References

[1] Frikha M, Nouri H, Guessasma S, Roger F and Bradai C 2017 Interfacial behavior from pull-out tests of steel and aluminium fibres in unsaturated polyester matrix *J. Mater. Sci.* **52** 13829-40
[2] Mouritz A P, Gellert E, Burchill P and Challis K 2001 Review of advanced composite structures for naval ships and submarines *Composite Structures* **53** 21-42
[3] Nikhamkin M, Sazhenkov N and Samodurov D 2017 Fatigue fracture of fiber reinforced polymer honeycomb composite sandwich structures for gas turbine engines *J. Phys.: Conf. Ser.* **843** 012029
[4] Bagherpour S 2012 *Fibre Reinforced Polyester Composites Intech* doi:10.5772/48697
[5] Zhandarov S F and Pisanova E V 1997 The local bond strength and its determination by fragmentation and pull-out tests *Composites Science and Technology* **57** 957-64
[6] Banholzer B, Brameshuber W and Jung W 2006 Analytical evaluation of pull-out tests-the

inverse problem *Cement & Concrete Composites* **28** 564-71
[7] Marotzke C and Qiao L 1997 Interfacial crack propagation arising in single-fiber pull-out tests *Composites Science and Technology* **57** 887-97
[8] Pisanova E, Zhandarov S, Mäder E, Ahmad I and Young R J 2001 Three techniques of interfacial bond strength estimation from direct observation of crack initiation and propagation in polymer-fibre systems *Composites: Part A* **32** 435-43
[9] Zhandarov S and Mäder E 2005 Characterization of fiber/matrix interface strength: applicability of different tests, approaches and parameters *Composites Science and Technology* **65** 114-60
[10] Scheer R J and Nairn J A 1995 A comparison of several fracture mechanics methods for measuring interfacial toughness with microbond tests *The Journal of Adhesion* **53** 45-68
[11] Wang C 1997 Fracture mechanics of single-fibre pull-out test *Journal of Materials Science* **32** 483-90
[12] Tsai K-H and Kim K-S 1996 The micromechanics of fibre pull-out *Journal of the Mechanics and Physics of Solids* **44** 1147-77
[13] Atkinson C, Avila J, Betz E and and Smelser R E 1982 The rod pull out problem, theory and experiment *Journal of the Mechanics and Physics of Solids* **30** 97-120
[14] Noda N-A, Wang Q, Uemura Y and Kawashima Y 1998 Singular integral equation method in the analysis of interaction between rectangular inclusions *JSME International Journal Series A: Mechanics and Material Engineering* **41** 303-8
[15] Chen D H and Nisitani H 1993 Singular stress field near the corner of jointed dissimilar materials *Journal of Applied Mechanics, Transactions ASME* **60** 607-13
[16] Chen D H and Nisitani H 1992 Analysis of intensity of singular stress field at fibre end (2nd Report, Results of Calculation) *Transactions of the Japan Society of Mechanical Engineers, Series A* **58** 143-8
[17] Miyazaki T, Noda N-A, Li R, Uchikoba T and Sano Y 2013 Debonding criterion for single lap joints from the intensity of singular stress field *Journal of the JIEP* **16** 143-51
[18] Miyazaki T, Noda N-A, Uchikoba T, Li R and Sano Y 2014 Proposal of a convenient and accurate method for evaluation of debonding strength *Transaction of the JSAE* **45** 895-901
[19] Carpenter W C and Byers C 1987 A path independent integral for computing stress intensities for V-notched cracks in a bi-material *International Journal of Fracture* **35** 245-68
[20] Bogy D B 1968 Edge-bonded dissimilar orthogonal elastic wedges under normal and shear loading *Trans ASME J Appl. Mech*. **35** 460-6
[21] Bogy D B 1971 Two edge-bonded elastic wedges of different materials a nd wedge angles under surface tractions *Trans ASME J Appl. Mech*. **38** 377-86
[22] Noda N A, Shirao R, Li J and Sugimoto J-S 2007 Intensity of singular stress fields causing interfacial debonding at the end of a fiber under pullout force and transverse tension *International Journal of Solids and Structures* **44** 4472-91
[23] Noda N-A, Suryadi D, Kumasaki S, Sano Y and Takase Y 2015 Failure analysis for coming out of shaft from shrink-fitted ceramic sleeve *Engineering Failure Analysis* **57** 219-35
[24] Noda N-A, Miyazaki T, Li R, Uchikoba T and Sano Y 2015 Debonding strength evaluation in terms of the intensity of singular stress at the interface corner with and without fictitious crack *Int. J. Adhes. Adhes* **61** 46-64
[25] Noda N-A, Uchikoba T, Ueno M, Sano Y, Iida K, Wang Z and Wang G 2015 Convenient debonding strength evaluation for spray coating based on intensity of singular stress *ISIJ International* **55** 2624-30
[26] Wang Z, Noda N-A, Ueno M and Sano Y 2016 Optimum design of ceramic spray coating evaluated in terms of intensity of singular stress field *Steel Research International* **88** 1600353
[27] Miyazaki T, Noda N-A, Ren F, Wang Z, Sano Y and Iida K 2017 Analysis of intensity of singular stress field for bonded cylinder and bonded pipe in comparison with bonded plate *Int. J. Adhes. Adhes.* **77** 118-37

[28] Noda N-A, Chen X, Sano Y, Wahab M A, Maruyama H and Fujisawa R 2016 Effect of pitch difference between the bolt-nut connections upon the anti-loosening performance and fatigue life *Materials and Design* **96** 476-89
[29] Noda N-A, Takase Y and Iizuka T 2005 Generalized stress intensiy factors at the fibre end in fibre reinforced plastics *Transactions of the JSME* **71** 36-42
[30] Marotzke C 1993 Influence of the fiber length on the stress transfer from glass and carbon fibers into a thermoplastic matrix in the pull-out test *Comp. Interfaces* **1** 153-66